PHYSICAL REVIEW B **82**, 224417 (2010)

Dipolar spin waves of lateral magnetic superlattices

P. Saraiva and A. Nogaret*
Department of Physics, University of Bath, Claverton Down, Bath BA2 7AY, United Kingdom

J. C. Portal†
High Magnetic Field Laboratory, 25 Avenue des Martyrs, 38042 Grenoble, France

H. E. Beere and D. A. Ritchie
Cavendish Laboratory, University of Cambridge, Cambridge CB3 0HE, United Kingdom

(Received 10 October 2010; revised manuscript received 26 November 2010; published 17 December 2010)

We investigate the high-frequency dynamics of dysprosium and cobalt gratings fabricated at the surface of a GaAs/$Al_{0.33}Ga_{0.67}As$ heterojunction. We detect the collective and localized spin-wave modes of the grating by measuring the photovoltage and the photoresistance induced in the two-dimensional electron gas (2DEG). The magnetic excitations couple to the 2DEG through their stray magnetic field. We perform a spectroscopy of dipolar-exchange spin waves as a function of microwave power, temperature, the tilt angle of the applied magnetic field, and by varying the structural and material parameters to change the strength of dipolar interactions. The data reveal two types of spin waves. Dipolar magnetization waves propagate across the grating through the magnetostatic interaction between the stripes. We derive an analytical expression of their dispersion curve and obtain a good fit of the ferromagnetic resonance broadening from first principles. The second type is dipolar edge spin waves which manifest through a series of sharp resonances at lower magnetic field. These waves are confined near the pole surfaces and interact very little with neighboring stripes. We calculate the eigenfrequencies of the quantized modes and obtain a qualitative explanation of the low-field resonances. The fit yields a value of the exchange stiffness constant of dysprosium, $A=1.5\times10^{-12}$ J m^{-1}. Our experiments show that photovoltage measurements in hybrid semiconductor-ferromagnetic structures provide a sensitive and noninvasive tool for probing the spin waves of small magnets (10–500 nm).

DOI: 10.1103/PhysRevB.82.224417 PACS number(s): 76.50.+g, 75.30.Ds, 73.23.−b

I. INTRODUCTION

Dipolar magnetic interactions are increasingly relevant to controlling the magnetization state of ultrasmall magnetic elements. Magnetostatic interactions control the nucleation field of magnetic vortices,[1] the magnetization state of nanowires[2,3] and notoriously increase cross-talk between bits as the size of magnetic memories is scaled down. Magnetic coupling can be used to a constructive effect in spin torque oscillators. The synchronization of spin-torque oscillators by spin waves (SWs) increases the power of microwave emission.[4–6] The study of magnetic dipolar interactions has recently been facilitated by the use of lithographic techniques to obtain rectangular prism magnets. Such magnets can be made small enough to have uniform magnetization and close enough to have strong mutual interactions.[7] At microwave frequencies, the edges of the prism reflect spin waves which leads to the formation of standing modes. Their absorption spectrum has been studied by Brillouin light scattering,[8,9] magnetoimpedance measurements,[10] and by microwave transmission through striplines.[11] The spectrum of spin waves is also modified by the presence of magnetic poles. The dipolar magnetic field creates spin wave quantum wells which bind dipolar edge SWs (DESWs).[12,13] The confinement of spin waves by magnetic quantum wells,[9] magnetic tunneling barriers,[14] periodic arrays,[15–17] and in Bose-Einstein condensates[18] has been investigated.

In this paper we demonstrate the formation of dipolar magnetization waves (DMWs) in one-dimensional (1D) superlattices. These waves propagate the displacement of the magnetization from one stripe to the next through pure magnetostatic interaction. We obtain the energy dispersion curve of DMWs in a simple form that generalizes the Kittel formula[19] of ferromagnetic resonance (FMR). In order to vary the coupling between stripes, we make dysprosium and cobalt gratings whose pitch we vary between 400 and 300 nm. We irradiate the gratings with microwaves and use a high mobility two-dimensional electron gas (2DEG) as a sensor of the stray magnetic field emanating from the grating. The high-frequency reversal of resonating magnetic dipoles was picked up in the photoresistance and the photovoltage induced across the 2DEG. We observe the formation of dipolar magnetization waves through the broadening of the ferromagnetic resonance. We find that the width of the ferromagnetic resonance (up to 1.5 T) is in quantitative agreement with the width of the DMW dispersion curve calculated using nominal structural and material parameters. We also report a series of small resonant dips at lower magnetic field. These present several of the characteristics expected from quantized DESWs. The number of DESW modes confined in each stripe yields the spin exchange stiffness constant. The value that we find is consistent with the one derived from the dispersion curve of magnons in bulk dysprosium.[20] We calculate the magnetic field dependence of the DESW eigenfrequencies and obtain a qualitative agreement with the experiment. We find that resonances are shifted to lower magnetic field by the magnetocrystalline anisotropy of ferromagnetic dysprosium. The height of the pho-

tovoltage peaks gives the stray magnetic field emanating from each type of spin wave. This magnetic field couples magnetic elements, hence from the height of the peak we are able to verify the localized or extended nature of spin-wave modes. Hybrid semiconductor-ferromagnetic structures are particularly well suited for probing ultrasmall magnets (10–500 nm). These are magnets which are smaller than the diffraction limit of Brillouin light scattering[16] and smaller than the minimum sample volume required for detecting ferromagnetic resonance.[21] The present photovoltage technique allows measuring the high-frequency dynamics of individual bits stored in magnetic dots tens of nanometers in size. High-frequency photovoltage measurements are able to detect changes in the magnetic moment as small as the Bohr magneton. This sensitivity can easily be verified using the Lenz law and is three orders of magnitude higher than the sensitivity achieved through ballistic Hall magnetometry in the static regime.[22]

The paper is organized as follows. Section I introduces the background. Section II reports on the ferromagnetic resonance of individual stripes (Co, Dy). These data provide a benchmark for the demonstration of the effects of dipolar coupling in gratings. Section III investigates the high-frequency dynamics of ferromagnetic gratings. Section IV develops the theory used to fit the DMW and DESW resonances. Section V discusses the findings, the approximations used, and the eventual shortcomings of the theory.

II. INDIVIDUAL FERROMAGNETIC STRIPES

Hybrid ferromagnetic-semiconductor devices were fabricated from a $GaAs/Al_{0.33}Ga_{0.67}As$ single heterojunction. The mobility and density of the 2DEG were determined from quantum transport measurements as $\mu=1.5\times10^6$ cm^2 V^{-1} s^{-1} and $n_s=1.6\times10^{11}$ cm^{-2}. We prepared Hall bars 8 μm wide and 32 μm long by optical lithography. Voltage probes were separated by distances ranging between 2 and 16 μm. Ferromagnetic gratings and individual stripes were then fabricated at the center of Hall bars to modulate the 2DEG located 80 nm below the surface—see Fig. 1. Magnetic modulations obtained in this way have an amplitude ~0.1 T. The perpendicular component of the stray magnetic field deflects ballistic trajectories in the 2DEG, coupling the electric properties of the 2DEG to the magnetic properties of the grating.[7] We have studied the four types of devices listed in Table I.

Samples of type *A* had a single dysprosium (or cobalt) stripe shown in Fig. 1(c). Samples *B*-*D* were 1D arrays such as the one shown in Fig. 1(b). The use of gratings of different pitch allows varying dipolar coupling and studying its effect on the high-frequency dynamics. Dysprosium was used because it has the highest magnetic moment per atom which maximizes the coupling between stripes. The tabulated values of the saturation magnetization at 4 K are $\mu_0 M_s=3.67$ T (Dy) and $\mu_0 M_s=1.84$ T (Co). In all devices, the stripes exceeded the length of the Hall bar by 10 μm at each end and effectively behaved as stripes of infinite length. Similarly, the gratings overlapped the active area of the Hall bar plus 10 μm on each side. The lack of edge effects allowed us to consider the grating as being infinite.

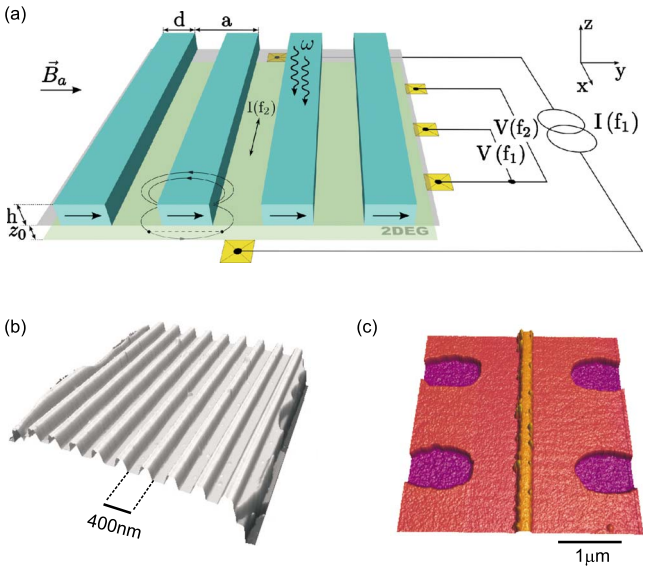

FIG. 1. (Color online) (a) Lateral superlattice consisting of an array of ferromagnetic stripes (Dy or Co) at the surface of a 2DEG. The grating is irradiated by microwaves at frequency ω while being magnetized in the plane by magnetic field B_a. At resonance, oscillations of the stray magnetic field induce a microwave current, $I(f_2)$, in the 2DEG. The photovoltage, $V(f_2)$ is measured at the frequency used to modulate the microwave power, $f_2=870$ Hz. The photoresistance is measured at frequency $f_1=30$ Hz. (b) Sample *B*: Dy grating, $a=400$ nm, $d=200$ nm, $h=160$ nm, and $z_0=80$ nm. (c) Sample *A*: Dy stripe, $d=200$ nm, $h=150$ nm, and $z_0=80$ nm.

Microwaves were generated by a range of backward wave oscillators covering the 35 GHz–110 GHz band. An overmoded circular waveguide carried unpolarized microwaves down to the sample space at the center of a 15 T superconducting magnet. The grating was irradiated at normal incidence while being magnetized by the external magnetic field, B_a—see Fig. 1(a). By tilting B_a in the plane of the 2DEG we were able to magnetize the stripes $\|y$ or $\|x$ to switch the dipolar magnetic field ON or OFF. When $B_a\|y$, magnetic poles form on the facets $\perp y$ and generate a spatially varying magnetic field. This magnetic field has two components $H_{d,y}$ and $H_{d,z}$. The $H_{d,z}$ component transmits high-frequency oscillations of the magnetization to the 2DEG by inducing eddy currents $I(f_2)$. The photovoltage and the photoresistance are measured using a double frequency modulation technique—see Fig. 1(a). One lock-in amplifier picks up the photovoltage $V(f_2)$ at frequency $f_2=870$ Hz which is used to modulate the microwave power. A second lock-in amplifier

TABLE I. Device parameters. Dimensions are in nanometer.

Sample	*A*	*B*	*C*	*D*
Magnet	Dy,Co stripe	Dy grating	Dy grating	Co grating
a		400	300	400
d	200	200	210	200
h	150	160	80	150
z_0	80	80	80	80

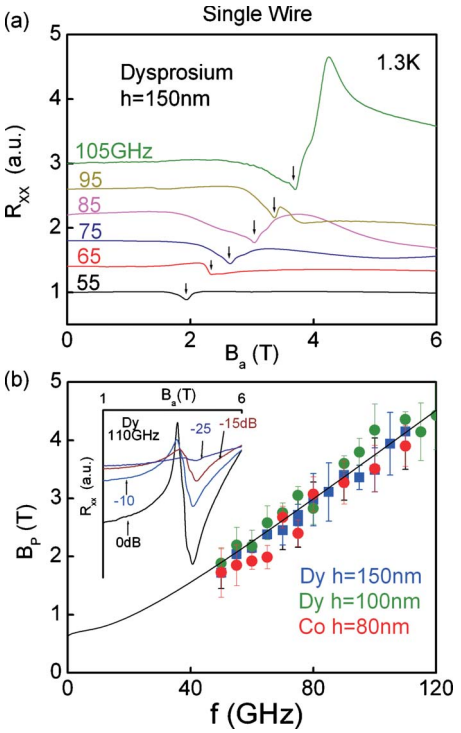

FIG. 2. (Color online) (a) Ferromagnetic resonance of sample *A* detected through a change in the resistance of the 2DEG ($B_a \| y$). Curves are vertically offset for clarity. (b) Frequency dependence of the resonant field (symbols) fitted with Eq. (1) (full line). Inset: microwave power dependence.

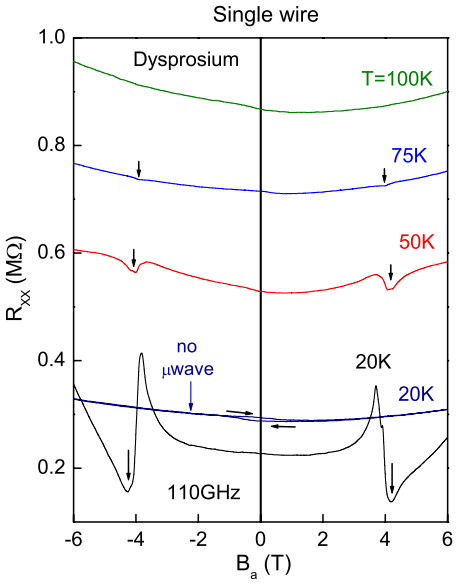

FIG. 3. (Color online) Temperature dependence of the photoresistance of sample *A*. The FMR vanishes above the Curie temperature of dysprosium (85 K). The magnetic hysteresis of dysprosium is visible in the curves measured without microwaves. Other curves are measured by sweeping the magnetic field up.

detects the longitudinal voltage $V(f_1)$ induced by a current drive $I(f_1)$ alternating at frequency $f_1=30$ Hz. The photoresistance was calculated as $R_{xx}=V(f_1)/I(f_1)$. We emphasize that B_a has no direct effect on electron ballistics in the 2DEG because it lies in the plane. In practice, a small misalignment is unavoidable. Using Hall voltage measurements, we estimate the residual perpendicular component to be 40 mT when the total external field is 3 T. This is smaller than the modulation field.

We now focus on the high-frequency dynamics of sample *A*. Under microwave irradiation, the magnetoresistance exhibits a single sharp resonance that moves to higher magnetic field with increasing microwave frequency—see Fig. 2(a). The position of the resonant dip depends linearly on the microwave frequency—see Fig. 2(b). The frequency dependence of ferromagnetic resonance generally follows the Kittel[19] formula,

$$\omega = \gamma\mu_0\{[H_a^* + (N_x - N_y)M_s][H_a^* + (N_z - N_y)M_s]\}^{1/2}, \quad (1)$$

where γ is the gyromagnetic ratio. $N_x=0$, $N_y=0.45$, $N_z=0.55$ are the demagnetization factors of the stripe derived from Rhodes and Rowlands[23,24] in Appendix A. We find that Eq. (1) must include the crystal-field anisotropy of Dy to fit the data which appear shifted to lower field. Magnetocrystalline anisotropy behaves as an internal magnetic field $\bar{H}_h$ that adds to H_a.[19] We therefore define the effective applied magnetic field as $H_a^*=H_a+\bar{H}_h$. The best fit is obtained for $\mu_0\bar{H}_h=0.6$ T—see Fig. 2(b) (full line). One obtains the Landé *g* factors $g=1.81$ (Co) and $g=1.95$ (Dy). Broad peaks are known to characterize the ferromagnetic resonance of dysprosium crystals.[25,26]

To demonstrate that the resonance is microwave induced, we study its power dependence in the inset to Fig. 2(b). To demonstrate that the resonance occurs in the ferromagnet—rather than in the 2DEG—we study its temperature dependence in Fig. 3. The peak amplitude decreases from 20 to 75 K and completely vanishes at 100 K. Since dysprosium is ferromagnetic up to 85 K, this explains the photoresistance resonance in this temperature range. Above 85 K, the magnetic moments adopt a spiral structure which produces zero net magnetization. Ferromagnetic resonance then becomes impossible which is why the resonant structure vanishes from the 100 K photoresistance curve. We have therefore demonstrated that the 2DEG is sensitive to the dynamics of small magnetic elements at its surface. In the case of individual stripes, the FMR occurs at a single frequency.

III. 1D FERROMAGNETIC GRATINGS

Magnetic gratings exhibit more complex magnetic excitations than single stripes. This can be seen in Fig. 4 which studies the photovoltage of sample *B* at microwave frequencies varying between 35 and 110 GHz. A series of complex resonances loosely delimited by the dashed lines replaces the single resonance of individual stripes. To allow for a more precise comparison with theory, we plot the onset and the end of the FMR range as the red (gray) and black circles in Fig. 5(a). The onset and the cut-off magnetic fields are taken at the half height of the FMR range—see Fig. 5(b). The FMR bandwidth increases with microwave frequency. It starts from 0.4 T at 35 GHz and increases to 1.8 T at 110 GHz.

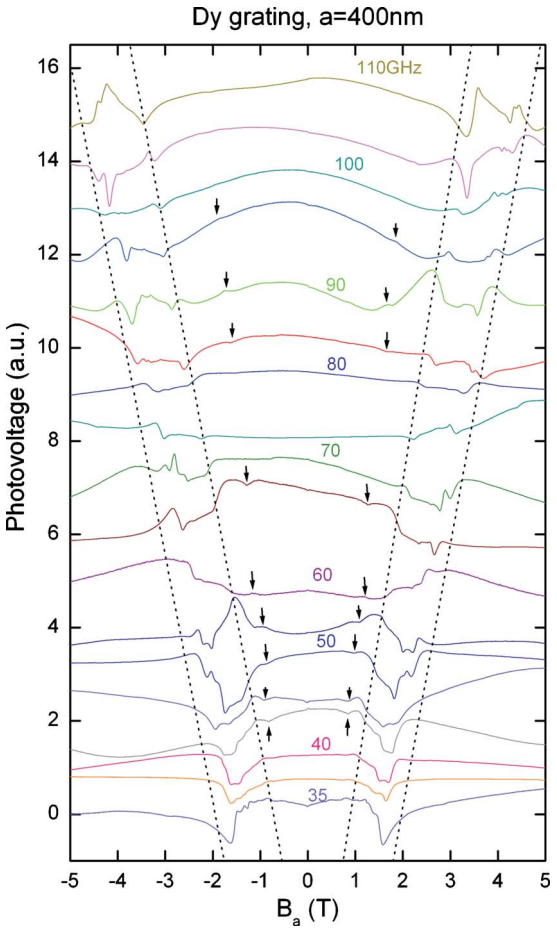

FIG. 4. (Color online) Photovoltage spectroscopy of magnetic excitations in sample B ($B_a \| y$). The dotted lines are a guide to the eyes for the magnetic field dependence of the onset and the cutoff of the FMR range. At lower magnetic field, the arrows indicate a series of smaller dips induced by microwaves. Curves are vertically offset for clarity. $T=1.3$ K.

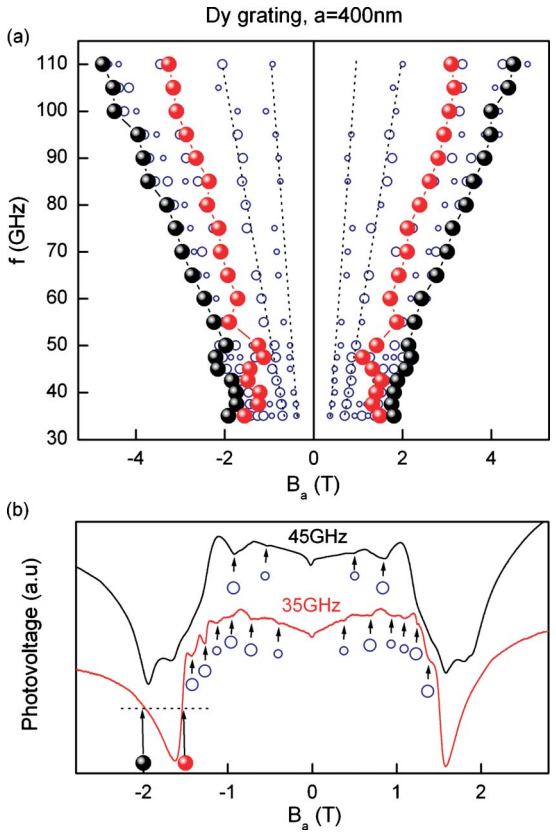

FIG. 5. (Color online) (a) Frequency dependence of the microwave resonances in the photovoltage of sample B. The fan diagram shows the FMR onset (red dots), the FMR cutoff (black dots), and the dependence of the small photovoltage dips at low field (blue open circles). (b) Details of the fine resonant structure at 35 and 45 GHz. The diameter of the blue circles is proportional to the amplitude of the dips. The onset (red dot) and the end (black dot) of the FMR range are defined at the midheight of the main resonance.

Below 60 GHz, the onset oscillates between the trend line and a higher magnetic field limit before settling on the higher magnetic field limit at 42 GHz. In comparison, the oscillations of the cutoff are weaker and remain centered on the trend line. It is believed that below 60 GHz, the magnetic field applied at the FMR onset minus the demagnetizing field becomes smaller than the field needed to saturate the magnetization ~1 T. This is why below 42 GHz, the FMR only survives at the higher end of the resonance range where the magnetization is more likely to be saturated.

Microwaves also induce a series of discrete resonances at lower magnetic field. These are indicated by the arrows in Fig. 4 and by the open circles in Fig. 5. The resonances shift linearly with frequency but at a weaker rate than the FMR. The narrowness of the dips and their occurrence below the FMR is suggestive of localized spin waves. There are two such localized modes in sample B.

Turning now to sample C, the photovoltage curves of Fig. 6 show a broadening of the FMR band, as in sample B. The FMR band hosts a complex series of subsidiary resonances. We plot the frequency dependence of the onset and the end of the FMR in Fig. 7(a). The width of the FMR increases from 0.9 T at 35 GHz to 1.4 T at 80 GHz thus qualitatively reproducing the trend of sample B. Unlike sample B however, the width of the FMR is more stable, less dependent on microwave frequency, below 60 GHz. This is one indication that dipolar interactions are more effective in stabilizing the magnetization in the direction perpendicular to the stripes. This allows the full FMR band to be observed at lower microwave frequencies than in sample B. The stronger coupling between stripes in sample C is also implied by the broader FMR, when compared to sample B. At 80 GHz, the FMR band is 1.4 T wide in sample C and 1.0 T in sample B.

Sample C exhibits a series of microwave induced dips below the FMR. The dips are indicated by the arrows in Fig. 6 and by the open circles in Fig. 7(a). Their frequency dependence is similar to that of the low-field resonances in sample B. However, there are three resonances in C compared to two in B. The first resonance occurs earlier, at $B_a=0.23$ T (C) compared to $B_a=0.39$ T (B) at 35 GHz. These data show that spin waves are more tightly confined in sample B than in C. Lateral confinement by the physical edges can be ruled out as an explanation, first because h is twice larger in sample B. The quantization of wave vector $q_z=p\pi/h$ gives the largest gaps in sample C—the opposite of

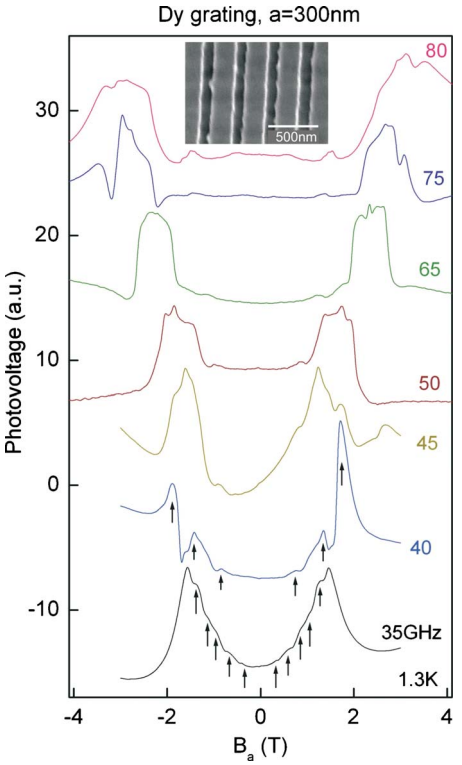

FIG. 6. (Color online) Photovoltage spectroscopy of magnetic excitations in sample C ($B_a \| y$). The broad FMR peak corresponds to the excitation of DMWs across the grating. The series of dips highlighted by the arrows indicates resonances with quantized DESW modes in individual stripes. Curves are vertically offset for clarity. Inset: dysprosium grating of sample C (detail).

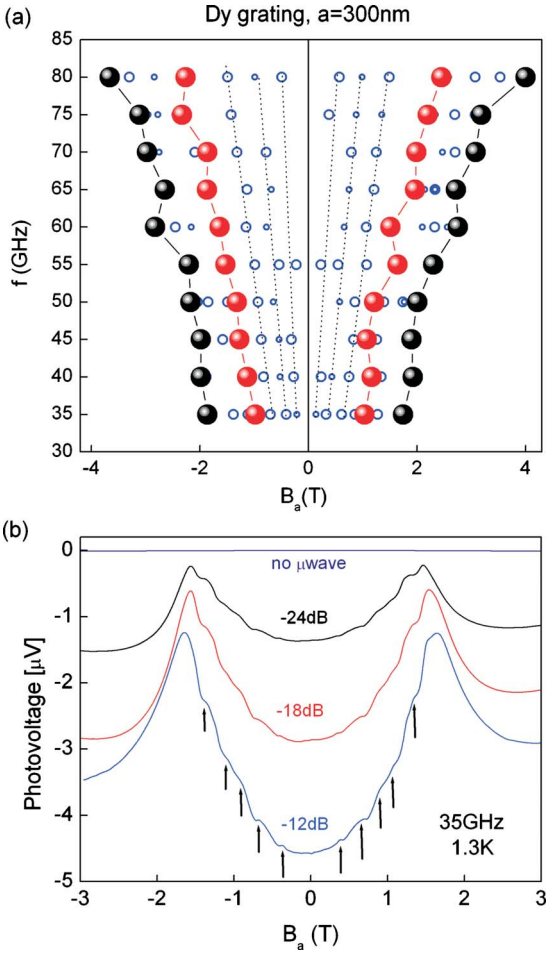

FIG. 7. (Color online) (a) Frequency dependence of the microwave resonances in the photovoltage of sample C. The fan diagram shows the FMR onset (red dots), the FMR cutoff (black dots), and the frequency dependence of the small photovoltage dips at low field (blue circles). (b) Detail of the 35 GHz curves showing the resonances with DESW modes and their dependence of microwave power.

what is observed. Second, the nearly identical values of d in B and C also rules out the quantization of q_y. The resonant dips must therefore arise from (magnetic) confinement in the y direction. The tighter spin-wave confinement in C is consistent with our earlier report of a stronger dipolar magnetic field in C.

Figure 8(a) maps the FMR signal detected in the resistance of sample D. The FMR band is 0.75 T wide at 80 GHz—see Fig. 8(b). This is smaller than in samples C(1.0 T) or B(1.4 T). In Appendix B, we calculate the dipolar magnetic field in the grating and show that it is proportional to the magnetization. Since the magnetization of Co is half that of Dy, the data demonstrate that the width of the FMR increases with the strength of the dipolar magnetic field.

We find that the photoresistance is highly anisotropic when the magnetic field is rotated in the plane—see Fig. 9. When the stripes are magnetized along their long axis, the 2DEG effectively decouples from the grating. The magnetoresistance remains featureless even at the highest microwave power and almost no change is observed when microwaves are switched off. An examination of the more sensitive photovoltage curves reveals a residual FMR signal and no resonant dips at lower field. Magnetizing the stripes along x eliminates the magnetic poles. This has three consequences: the stripes decouple from each other, the grating decouples from the 2DEG and the confinement of surface spin waves vanishes. The latter explains the absence of resonant dips in the photovoltage curves. Under resonant conditions with $B_a \| x$, the oscillations of magnetization components M_y and M_z induce stray rf magnetic fields at the site of the 2DEG. The small amplitude of the photovoltage peaks and the absence of any effect in the photoresistance suggests that the ferromagnetic resonance cone is very narrow, M_y, $M_z \ll M_s$. We now develop a theory that incorporates the above ideas and use it to fit the experiments.

IV. THEORY

We start by calculating the magnetic field emanating from an infinite array of rectangular stripes whose stripes are assumed to be uniformly magnetized along y. Maxwell's equations are solved using Fourier analysis in Appendix B. We obtain the $H_{d,y}$ and $H_{d,z}$ vector components in the analytical form of Eqs. (B3) and (B4). We compute their spatial variation in the case of superlattice C and plot it in Fig. 10. Be-

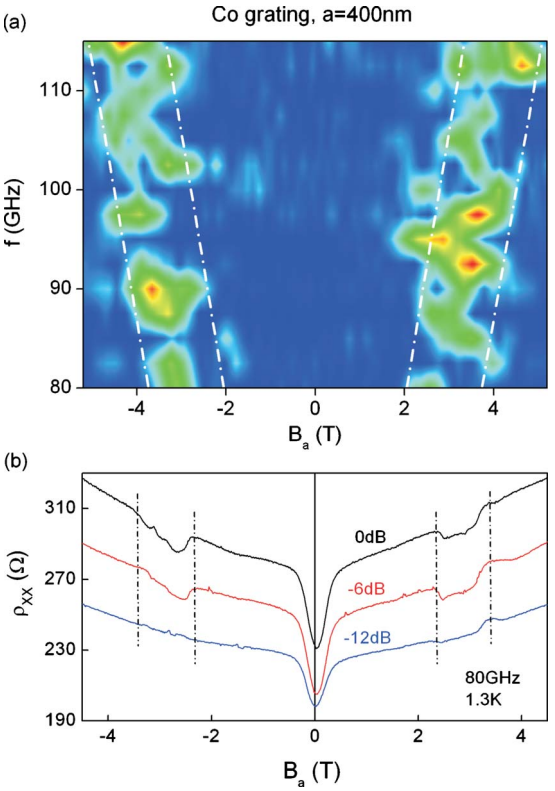

FIG. 8. (Color online) (a) Photoresistance of sample *D* mapped as a function of microwave frequency and magnetic field ($B_a \| y$). The bandwidth of the resonance with DMWs is delimited by the dashed-dotted lines. (b) Microwave power dependence.

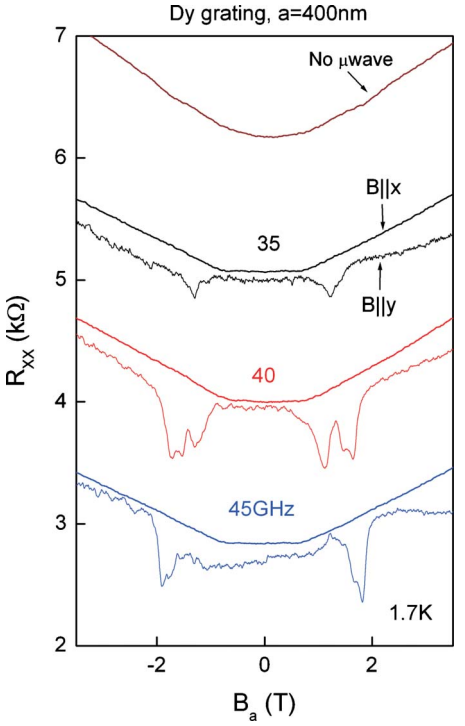

FIG. 9. (Color online) Comparison of the photoresistance obtained in a transverse magnetic field ($B_a \| y$) and a longitudinal magnetic field ($B_a \| x$) for sample *B*. When $B_a \| x$, the dipolar magnetic field is zero. Resonant absorption is recovered by aligning $B_a \| y$.

tween $-d/2$ and $+d/2$, $H_{d,y}$ is the demagnetizing magnetic field of the stripe. This field is strongly inhomogeneous decreasing from -0.4 T at the center to -1.4 T near the poles. By contrast, $H_{d,y}$ varies smoothly in the z direction away from the $z=0$ plane. Note that the magnetic well at $\pm d/2$ extends vertically right up to the physical edge of the stripe at $z=h/2$, making magnetic confinement undistinguishable from physical confinement in this direction. In panel (b), $H_{d,z}$ diverges at the corners of the stripe. This is where the magnetic flux flips by 180°. $H_{d,z}$ decays exponentially away from the stripes, giving a sinusoidal modulation of amplitude 0.24 T as it passes through the plane of the 2DEG.

Prior to modeling dipolar spin waves in confined geometries, it is necessary to recall the properties of bulk spin waves in ferromagnetic dysprosium. When H_a is along the magnetic easy axis—*a* axis—the energy dispersion curve is given by[27]

$$\hbar\omega(\mathbf{q}) = \{[2S[J(0) - J(\mathbf{q})] + 3K_2S^{-1} + \hbar\gamma\mu_0 H_a][2S[J(0) - J(\mathbf{q})] + 36K_6^6 S^{-1} + \hbar\gamma\mu_0 H_a]\}^{1/2}, \quad (2)$$

where $S=15/2$ is the angular momentum on each Dy ion, $J(\mathbf{q})$ is the Fourier transform of the exchange interaction. The energy width of the magnon dispersion curve relates to the exchange energy of dysprosium $\Delta E_{exch} \cong 7$ meV.[20] $K_2 = 87\times10^6$ J m^{-3} and $K_6^6 = -1.1\times10^6$ J m^{-1} are the axial and hexagonal energies of magnetocrystalline anisotropy[28] which measure the energy cost of aligning the magnetization along the *c*- and *b*-hard magnetic axes. The anisotropy terms in Eq. (2) behave as two effective magnetic fields: $\mu_0 H_c = 3K_2/(SM_s)$ (12 T) and $\mu_0 H_h = 36K_6^6/(SM_s)$ (1.8 T) which add to H_a.[19] Given the large value of the H_c field, magnetocrystalline anisotropy reduces to the effects of H_h: the FMR lines are shifted to lower magnetic field by $-H_h$ and there is a finite resonance frequency at zero magnetic field. Since our Dy stripes are polycrystalline,[29] the magnetic field assumes random orientations with respect to the *a* axis. We estimate the effective anisotropy of the polycrystal by averaging the $\sin^2\theta$ dependence of the magnetocrystalline energy over the solid angle of 4π radian. We obtain $\bar{H}_h = H_h/3$ (0.6 T) which is the offset magnetic field observed in our dysprosium devices.

A. Dipolar edge spin waves

We now calculate the frequencies of spin waves quantized by magnetic wells at $\pm d/2$ in Fig. 10(a). The calculation follows the method of Bayer *et al.*[8] The frequency dispersion of dipolar-exchange spin waves in a thin film[30] is

$$\left(\frac{\omega}{\omega_M}\right) = \left\{\left[\frac{\omega_H}{\omega_M} + \alpha q^2\right]\left[\frac{\omega_H}{\omega_M} + \alpha q^2 + \frac{1-\exp(-qh)}{qh}\right]\right\}^{1/2}, \quad (3)$$

where $\omega_M = \gamma\mu_0 M$, $\omega_H(y) = \gamma\mu_0[H_a + \bar{H}_h + H_{d,y}(y)]$, and $\alpha = 2\pi A/\mu_0 M_s^2$ is the exchange constant expressed as a function of A, the exchange stiffness constant. The wave vector $\mathbf{q} = q_x\mathbf{e_x} + q_y\mathbf{e_y} + q_z\mathbf{e_z}$ has two quantized components q_y and q_z

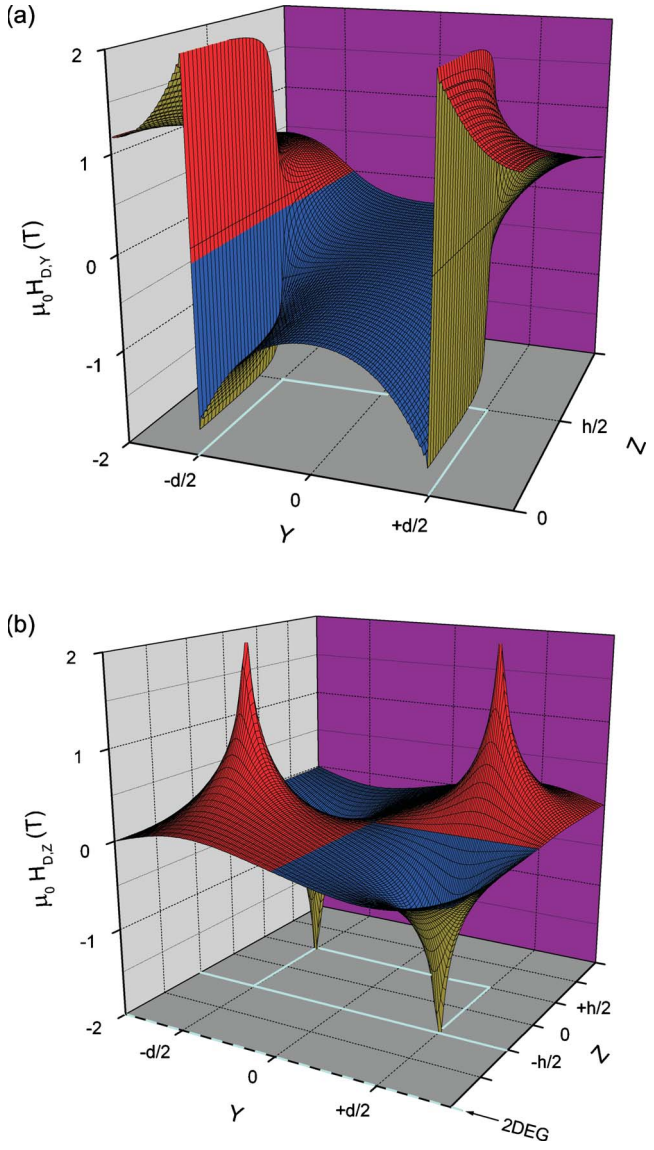

FIG. 10. (Color online) Spatial variation in the (a) in-plane and (b) perpendicular dipolar magnetic field in one stripe of superlattice C. The superlattice is assumed to be magnetized to saturation along y. The edges of the stripe are indicated by the full lines in the (y,z) plane. The magnetic field that couples the grating to the 2DEG is the sine wave at the fore of panel (b).

and one free component q_x. Wave vector $q_z = p\pi/h$, $p = 1,2,3,\ldots$ is quantized by the finite thickness of the film. Wave vector q_y is confined by the spatial variation of the internal magnetic field. When the Larmor frequency of the internal magnetic field is smaller than the microwave frequency, $\omega_H < \omega$, Eq. (3) admits real solutions in q which correspond to propagating waves. If the solutions are imaginary, spin waves are evanescent. Dipolar surface spin waves thus propagate near the poles where the internal magnetic field is the lowest. With the magnetic field profile behaving as a quantum well, the momentum q_y takes discrete values given by the Wentzel-Kramers-Brillouin quantization,[12]

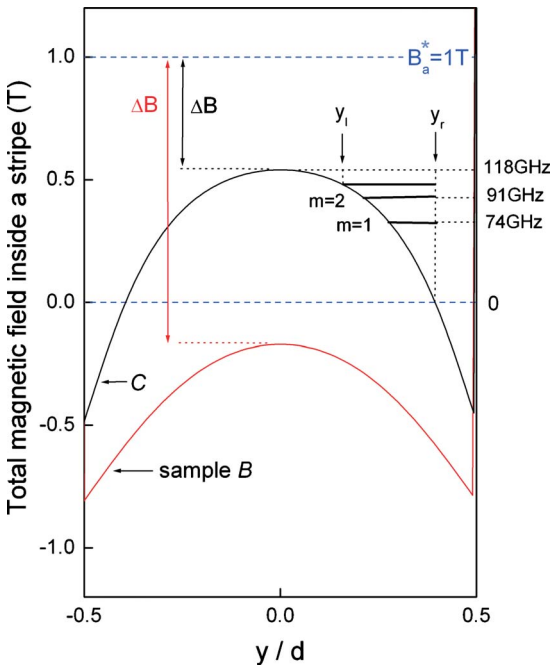

FIG. 11. (Color online) Internal magnetic field across one stripe at height $z=0$. The magnetic bias is $B_a + \bar{B}_h = 1$ T. ΔB is the bias threshold where the internal magnetic field becomes positive at the center of the stripes and starts squeezing spin waves against the edges. The quantized DESW modes $m=1$, 2, and 3 $(p=1)$ are shown together with their frequencies. y_l and y_r are the left and right turning points of the $m=3$ DESW mode.

$$\int_{y_l}^{y_r} q_y[H_d(y),\omega]dy = m\pi. \tag{4}$$

y_l and y_r are the left and right turning points shown in Fig. 11. For the magnetic well centered at $+d/2$, y_l is the point where spin waves become evanescent and y_r is where $\omega_H = 0$.

We proceed with the calculation by finding the wave vector q_m where the dispersion curve, Eq. (3), goes through its minimum. q_m depends only on the microwave frequency. By inserting q_m into Eq. (3) we find the internal magnetic field at the left turning point. The spatial variation in the dipolar magnetic field being known, we obtain y_l by solving Eq. (B3) numerically. The right turning point is obtained in a similar way by solving $\omega_H(y_r) = 0$. Once y_l and y_r are known, the frequencies of the quantized DESWs $m = 1,2,3,\ldots$ are calculated using Eq. (4). These modes are shown in Fig. 11. Their magnetic field dependence is plotted in Fig. 12.

We now comment on the theoretical magnetic field dependence of the DESW frequencies in Fig. 12. The theory agrees with the experiment on the following points. First, the DESW fan structure starts from a lower magnetic field in sample C than in sample B. This is because the demagnetizing field is stronger inside stripe C—see Fig. 11. As a result, the magnetic field ΔB needed to create a spin wave well is smaller in C than in B. Second, the theory obtains the correct number of trapped modes using $A = 1.5 \times 10^{-12}$ J m^{-1} as the spin exchange stiffness constant of dysprosium.[20] The ex-

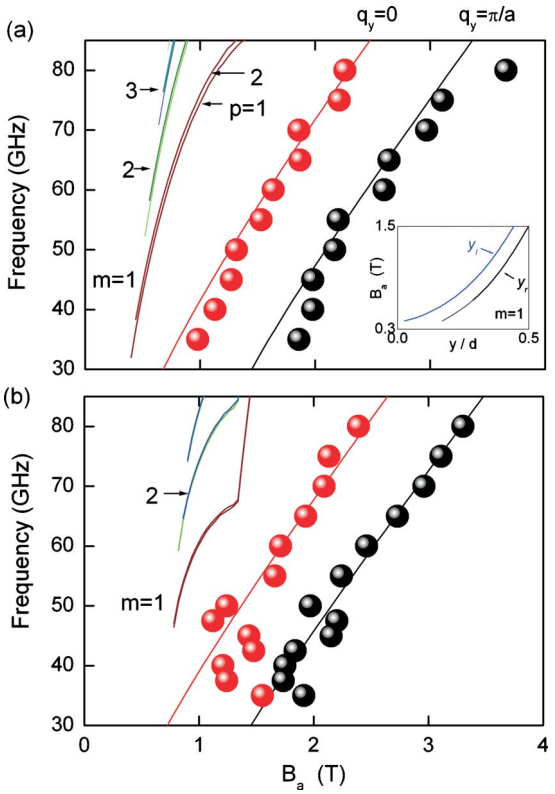

FIG. 12. (Color online) Theoretical frequency dependence of the DESW modes ($m=1,2,3,\ldots$, $p=1,2$) in samples (a) *C* and (b) *B*. The theoretical frequency dependence of the onset and cut-off magnetic fields of the DMW band is plotted as the red and black curves. Inset: left and right turning points of the $m=1$ DESW mode. This mode drifts toward the edge of the stripe as the magnetic field increases.

change constant calculated from $\alpha=2\pi A/\mu_0 M_s^2$ gave $\alpha=0.5$ nm^2. Third, the theory predicts one more branch in the theoretical fan of *C* than in the fan of *B*. This is consistent with the observation of an additional branch in the experimental fan of sample *C*. This difference is explained by the deeper spin wave well of sample *C*—see Fig. 11. Fourth, the theory correctly locates the DESW resonances below the FMR. Fifth, the frequency splitting of the $p=1$ and $p=2$ subbands induced by the vertical confinement is negligible compared to magnetic confinement along *y*.

The nonlinearity of the theoretical branches however prevents making a quantitative fit. The bend in the $m=1$ curve of panel (b) occurs when the right turning point of the first DESW mode collides with the pole surface. At this point, the tighter confinement results in an upward shift of the $m=1$ mode. The drift of this mode toward the pole surface is shown in the inset to Fig. 11. Possible ameliorations to this picture are discussed in Sec. V.

B. Dipolar magnetization waves

We now consider an infinite array of rectangular magnetic stripes and calculate the frequency dispersion curve of the DMWs, $\omega(q_y)$. The dephasing of the magnetization from one stripe to the next makes the coupling between stripes dependent on wave vector q_y. As a result, the grating becomes a dispersive medium for the magnetization waves that propagate through it. The DMW modes enter resonance over a finite range of frequencies which explains the FMR bandwidth. Since the FMR occurs in magnetic fields over 1 T, we consider the magnetization of Dy stripes to be saturated.

Consider one stripe labeled $n=0$. Its magnetization $\mathbf{M}^{(0)}$ experiences a torque from B_a as well as from the spatially varying magnetic field emanating from all stripes. With our assumption of a homogeneous magnetization, the overall torque applied to stripe $n=0$ is the torque exerted by the stray magnetic field averaged over the stripe ($\bar{\mathbf{B}}$). Under constant microwave irradiation, the magnetization obeys a gyroscopic equation of the form

$$\frac{d\mathbf{M}^{(0)}}{dt} = \gamma \mathbf{M}^{(0)} \wedge \bar{\mathbf{B}}(t), \tag{5}$$

where

$$\mathbf{B}(y,t) = \mu_0 \begin{cases} 0 \\ H_{d,y}(y,t) + H_a^* \\ H_{d,z}(y,t), \end{cases} \tag{6}$$

$\mathbf{H}_d$ is obtained from elementary magnetostatics[24,31] as the sum of the dipolar field from each stripe. The magnetization of stripe *n*, $\mathbf{M}^{(\mathbf{n})}(t)$, generates a dipolar magnetic field $H_{d,y}^{(n)}(y,t)=-N_y^{(n)}(y)M_y^{(n)}(t)$ and $H_{d,z}^{(n)}(y,t)=-N_z^{(n)}(y)M_z^{(n)}(t)$ at the locus of stripe 0. The coefficients $N^{(n)}$ are calculated at $z=0$ by neglecting the variation in the internal magnetic field in the *z* direction. This approximation is suggested by an examination of Fig. 10(a) and will be verified below. One obtains

$$N_y^{(n)}(y) = \frac{1}{\pi}\left\{\arctan\frac{1}{\zeta_n^+} - \arctan\frac{1}{\zeta_n^-}\right\}, \tag{7}$$

$$N_z^{(n)}(y) = \frac{1}{\pi}\{\arctan\,\zeta_n^+ - \arctan\,\zeta_n^-\}, \tag{8}$$

where $\zeta_n^{\pm}=(2y-2na\pm d)/h$. $N_x^{(n)}(y)=0$. The coupling coefficients are averaged to give the torque on stripe 0,

$$\bar{N}_\alpha^{(n)} = \frac{1}{d}\int_{-d/2}^{+d/2} dy N_\alpha^{(n)}(y) \quad \alpha \equiv (y,z). \tag{9}$$

If $n=0$, Eq. (9) gives the demagnetization coefficients of the semi-infinite prism. These satisfy the well-known sum rule $\bar{N}_x^{(0)}+\bar{N}_y^{(0)}+\bar{N}_z^{(0)}=1$. If $n>0$, the $\bar{N}_\alpha^{(n)}$ may be loosely viewed as generalized demagnetization coefficients arising from the coupling to other stripes. However $\bar{N}_y^{(n)}$ is negative whereas $\bar{N}_z^{(n)}$ is positive. These coefficients obey a new sum rule: $\bar{N}_x^{(n)}+\bar{N}_y^{(n)}+\bar{N}_z^{(n)}=0$ $(n>0)$. One calculates $\mathbf{H}_d$ by summing the contribution from all stripes. The result is inserted into Eqs. (5) and (6). We solve Eq. (5) by seeking solutions of the form $\mathbf{M}^{(\mathbf{n})}(t)=\mathbf{M}^{(\mathbf{0})}e^{i(q_y na-\omega t)}$. Using the symmetry property $\bar{N}_\alpha^{(n)}=\bar{N}_\alpha^{(-n)}$, one finds the dispersion curve of DMWs,

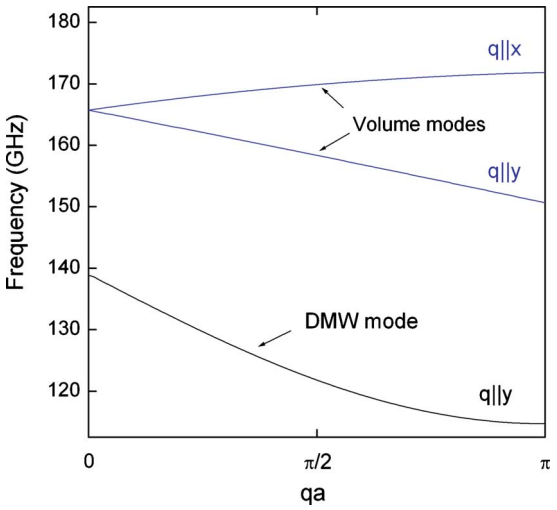

FIG. 13. (Color online) Frequency dispersion curve of dipolar magnetization waves in superlattice C at $B_a=5$ T. The volume spin-wave modes of a 80-nm-thick dysprosium film are also shown for the two directions of propagation, parallel $(q\|y)$ and perpendicular $(q\|x)$ to the magnetization.

$$\omega^2 = (\gamma\mu_0)^2\left\{H_a^* + \sum_{n=0}^{\infty} c_n[\bar{N}_z^{(n)} - \bar{N}_y^{(n)}]\cos(q_y na)M_s\right\} \times\left\{H_a^* - \sum_{n=0}^{\infty} c_n\bar{N}_y^{(n)}\cos(q_y na)M_s\right\}, \quad (10)$$

where $c_0=1$ and $c_n=2$ for $n\neq 0$. Equation (10) generalizes the Kittel formula of Eq. (1).[19] It makes clear that dispersive terms arise from the demagnetization coefficients of higher order $n>0$. The effects of long range dipolar coupling are particularly noticeable at long wavelengths where the frequency depends linearly on the wave vector—see Fig. 13. The group velocity of DMWs is negative because the $N_y^{(n)}$ are negative. At long wavelengths, the in-plane dipolar field reinforces the applied magnetic field. As a result the Larmor frequency is maximum at $q_y=0$. For comparison, we have also calculated the volume spin-wave modes[30] of the unpatterned Dy film which has the same thickness as sample C—see Fig. 13. The frequency offset between these modes and DMW modes at $q=0$ is due to the demagnetizing field in the patterned film.

Returning to the experimental data, the DMWs of wave vector $q_y=0$ are the first to enter resonance since they require the lowest magnetic field to oscillate at frequency ω. The DMW modes at $q_y=0$ $(q_y=\pi/a)$ are excited at the onset (cutoff) of the FMR range. The theoretical dependence of the FMR onset [red (gray) line] and the FMR cutoff (black line) is plotted in Fig. 12. The use of the nominal parameters of samples B and C gives a FMR linewidth and position in very good agreement with the experiment (dots). This demonstrates the formation of DMWs in superlattices.

V. DISCUSSION

Our results demonstrate the coexistence of two types of spin waves in magnetic superlattices. Dipolar magnetization waves are plane waves that travel across the superlattice. Dipolar edge spin waves, by contrast, are two-dimensional waves quantized by spin-wave quantum wells near pole surfaces. There is no experimental evidence suggesting the hybridization of DESWs across the superlattice. Judging the strength of the dipolar interaction by the height of the resonances, the coupling between DESWs in different stripes must be at least ten times smaller than the magnetostatic coupling between stripes. The experiment does not permit to ascertain whether DESWs trapped at opposite edges of the same stripe hybridize or not. Intrastripe coupling is predicted to be negligible at the high magnetic fields that we apply.[8] This seems to be confirmed by the absence of splitting of the dips at higher m values. The magnetic field dependence of these dips is more fanlike than the theory predicts.[32] This discrepancy comes from the assumption of a uniform magnetization which we made to calculate $\mathbf{H}_d$. This assumption has the effect of giving a strong demagnetization field between y_r and $+d/2$ which tends to create a magnetic domain. As a result, the magnetization and dipolar field must be computed self-consistently with the result that both the magnetization and the dipolar field decay smoothly to zero at $+d/2$. This correction to the model would make $y_r\approx d/2$ and eliminate the bend in the $m=1$ branch of Fig. 12(b).

Microwaves excite spin waves of finite momentum through two-magnon scattering. *A priori*, this process can excite either volume spin waves propagating in the direction of the magnetization $(q\|y)$ or DMWs. Both modes have similar dispersion curves with negative group velocity. The wave vector of backward volume modes will however be quantized by the edge of the stripes. The smallest allowed momentum $q_y=\pi/d$ is outside the Brillouin zone of the superlattice. We believe that the superlattice couples microwaves more efficiently to DMW modes than to volume modes because magnons at the lowest frequencies in the DMW spectrum can be excited with a much smaller momentum. The grating behaves as a two-dimensional coupler of magnons to microwaves in a similar way as at infrared frequencies.[33,34] Concerning volume modes propagating along the wire, Fig. 13 shows that their dispersion curve has a width of only 5 GHz which is too narrow to explain the observed FMR band. It also seems unlikely that these volume modes are excited together with DMW modes because no gap appears in the FMR spectrum. Therefore it can be argued that microwaves couple predominantly to DMW modes. From a pure experimental point of view, we believe that the FMR broadening is mainly due to dipolar coupling for the following reasons. First, samples B (Dy) and D (Co) have the same dimensions, yet the FMR of B is 1.4 times broader than that of D. Second, if one compares the resonance of individual Dy stripes (A) with those of a grating made of the very same stripes (B), one notices that A has a single resonant peak whereas B shows a "square" band incorporating a weaker substructure. If scattering by volume modes occurred in the grating, a resonant band would also be seen in the single stripes. Although the shape of resonances varies from sample to sample, the differences in resonance width is a constant feature that distinguishes the stripes from the arrays. We can therefore say with confidence that the broadening of the resonance in superlattices arises from in-

teractions between stripes. To be complete, we verify the assumption of the constancy of the internal field along z which we made when calculating the demagnetization coefficients $\bar{N}_\alpha^{(n)}$. Considering one stripe of sample B, the demagnetization factors calculated from Eq. (9) are $\bar{N}_y^{(0)}=0.49$ and $\bar{N}_z^{(0)}=0.51$. The exact demagnetization factors calculated from Eqs. (A1) and (A2) are $N_y=0.45$ and $N_z=0.55$. The small differences in these numbers show that Eq. (10) remains a good approximation of the dispersion curve even for relatively thick stripes.

In conclusion we have shown that photovoltage measurements in hybrid structures provide a highly sensitive and noninvasive probe of the magnetization dynamics. By sampling the stray magnetic field emanating from individual spin waves, we were able to demonstrate the formation of extended dipolar magnetization waves and localized edge spin waves in arrays of ferromagnetic stripes. Our technique complements established techniques by resolving the magnetization dynamics of ultrasmall magnets using micron size Hall junctions.

ACKNOWLEDGMENTS

This work was supported by the EPSRC (U.K.) under Grant No. EP/E002390/1. Access to magnetic field facilities was provided under the EU Transnational Access Contract No. 228043—Euromagnet II.

APPENDIX A: DEMAGNETIZATION FACTORS OF INFINITE STRIPES

Given a rectangular stripe of cross-sectional aspect ratio $k=h/d$, the demagnetization factors[23] are

$$N_y=\frac{1}{\pi k}\ln\left(\frac{1}{\sqrt{1+k^2}}\right)+\frac{k}{\pi}\ln\left(\frac{\sqrt{1+k^2}}{k}\right)+1-\frac{2}{\pi}\arctan\frac{1}{k}, \tag{A1}$$

$$N_z=\frac{k}{\pi}\ln\left(\frac{k}{\sqrt{1+k^2}}\right)+\frac{1}{\pi k}\ln(\sqrt{1+k^2})+1-\frac{2}{\pi}\arctan k. \tag{A2}$$

APPENDIX B: DIPOLAR MAGNETIC FIELD OF A 1D SUPERLATTICE

We obtain the magnetic field $\mathbf{H}$ emanating from the grating by solving the Maxwell's equations of magnetostatics $\nabla\cdot\mathbf{H}=-\nabla\cdot\mathbf{M}$ and $\nabla\wedge\mathbf{H}=0$. Consider one stripe centered on the origin whose magnetization M_y is homogeneous. The magnetization function defined across one period of the grating is

$$\mathbf{M}=\begin{cases}0\\ M_y\left[\theta\left(z-\frac{h}{2}\right)-\theta\left(z+\frac{h}{2}\right)\right]\left[\theta\left(y-\frac{d}{2}\right)-\theta\left(y+\frac{d}{2}\right)\right]\\ 0\end{cases},$$

where θ is the Heaviside step function. The magnetization function is step and repeated across the grating hence lending itself to Fourier analysis. The symmetry of the system and its invariance by translation along x imply that $\mathbf{H}=H_y(y,z)\mathbf{e_y}+H_z(y,z)\mathbf{e_z}$. The two Maxwell's equations are easily solved in Fourier space after making the transformation,

$$\mathbf{H}(y,z)=\sum_{n=-\infty}^{+\infty}\mathbf{H}(q_n,z)e^{-iq_ny}, \tag{B1}$$

$$\mathbf{H}(q_n,z)=\frac{1}{a}\int_{-a/2}^{+a/2}dy\mathbf{H}(y,z)e^{+iq_ny}, \tag{B2}$$

where $q_n=2\pi n/a$. We first obtain the Fourier coefficients $\mathbf{H}(q_n,z)$ then compute the stray magnetic field in real space using Eq. (B1). The in-plane vector component is

$$H_y(y,z)=-M_y\frac{hd}{a}\sum_{n=1}^{+\infty}q_nF_y(q_n,z)\cos(q_ny), \tag{B3}$$

where the form factor is

$$F_y(q_n,z)=\begin{cases}\dfrac{\sin\left(\frac{q_nd}{2}\right)}{\frac{q_nd}{2}}\dfrac{\sinh\left(\frac{q_nh}{2}\right)}{\frac{q_nh}{2}}e^{-q_n|z|} & |z|>\dfrac{h}{2}\\ \dfrac{\sin\left(\frac{q_nd}{2}\right)}{\frac{q_nd}{2}}\dfrac{1-e^{-q_nh/2}\cosh(q_nz)}{\frac{q_nh}{2}} & |z|<\dfrac{h}{2}\end{cases}.$$

The perpendicular vector component is

$$H_z(y,z)=+M_y\frac{hd}{a}\sum_{n=1}^{+\infty}q_nF_z(q_n,z)\sin(q_ny) \tag{B4}$$

with form factor

$$F_z(q_n,z)=\begin{cases}\dfrac{\sin\left(\frac{q_nd}{2}\right)}{\frac{q_nd}{2}}\dfrac{\sinh\left(\frac{q_nh}{2}\right)}{\frac{q_nh}{2}}\mathrm{sgn}(z)e^{-q_n|z|} & |z|>\dfrac{h}{2}\\ \dfrac{\sin\left(\frac{q_nd}{2}\right)}{\frac{q_nd}{2}}\dfrac{\sinh(q_nz)}{\frac{q_nh}{2}}e^{-q_nh/2} & |z|<\dfrac{h}{2}\end{cases},$$

where

$$\mathrm{sgn}(z)=\begin{cases}+1 & z>0\\ -1 & z<0\end{cases}.$$

*a.r.nogaret@bath.ac.uk
†Also at Institut Universitaire de France and Institut National des Sciences Appliquées, 31077 Toulouse, France.

[1] A. Vogel, A. Drews, T. Kamionka, M. Bolte, and G. Meier, Phys. Rev. Lett. **105**, 037201 (2010).
[2] J. De La Torre Medina, L. Piraux, J. M. Olais Govea, and A. Encinas, Phys. Rev. B **81**, 144411 (2010).
[3] U. Ebels, J.-L. Duvail, P. E. Wigen, L. Piraux, L. D. Buda, and K. Ounadjela, Phys. Rev. B **64**, 144421 (2001).
[4] S. Kaka, M. R. Pufall, W. H. Rippard, T. J. Silva, S. E. Russek, and J. A. Katine, Nature (London) **437**, 389 (2005).
[5] F. B. Mancoff, N. D. Rizzo, B. N. Engel, and S. Tehrani, Nature (London) **437**, 393 (2005).
[6] A. N. Slavin and V. S. Tiberkevich, Phys. Rev. B **72**, 092407 (2005).
[7] A. Nogaret, J. Phys.: Condens. Matter **22**, 253201 (2010).
[8] C. Bayer, J. Jorzick, S. O. Demokritov, A. N. Slavin, K. Y. Guslienko, D. V. Berkov, N. L. Gorn, M. P. Kostylev, and B. Hillebrands, in *Spin Dynamics in Confined Magnetic Structures III*, edited by B. Hillebrands and A. Thiaville (Springer, New York, 2006), Vol. 101.
[9] M. P. Kostylev, A. A. Serga, T. Schneider, T. Neumann, B. Leven, B. Hillebrands, and R. L. Stamps, Phys. Rev. B **76**, 184419 (2007).
[10] M. R. Britel, D. Ménard, L. G. Melo, P. Ciureanu, A. Yelon, R. W. Cochrane, M. Rouabhi, and B. Cornut, Appl. Phys. Lett. **77**, 2737 (2000).
[11] Y. S. Gui, N. Mecking, and C. M. Hu, Phys. Rev. Lett. **98**, 217603 (2007).
[12] J. Jorzick, S. O. Demokritov, B. Hillebrands, M. Bailleul, C. Fermon, K. Y. Guslienko, A. N. Slavin, D. V. Berkov, and N. L. Gorn, Phys. Rev. Lett. **88**, 047204 (2002).
[13] J. P. Park, P. Eames, D. M. Engebretson, J. Berezovsky, and P. A. Crowell, Phys. Rev. Lett. **89**, 277201 (2002).
[14] S. O. Demokritov, A. A. Serga, A. André, V. E. Demidov, M. P. Kostylev, B. Hillebrands, and A. N. Slavin, Phys. Rev. Lett. **93**, 047201 (2004).
[15] M. P. Kostylev, A. A. Stashkevich, and N. A. Sergeeva, Phys. Rev. B **69**, 064408 (2004).
[16] G. Gubbiotti, S. Tacchi, G. Carlotti, N. Singh, S. Goolaup, A. O. Adeyeye, and M. Kostylev, Appl. Phys. Lett. **90**, 092503 (2007).
[17] G. Gubbiotti, S. Tacchi, G. Carlotti, P. Vavassori, N. Singh, S. Goolaup, A. O. Adeyeye, A. Stashkevich, and M. Kostylev, Phys. Rev. B **72**, 224413 (2005).
[18] S. O. Demokritov, V. E. Demidov, O. Dzyapko, G. A. Melkov, A. A. Serga, B. Hillebrands, and A. N. Slavin, Nature (London) **443**, 430 (2006).
[19] C. Kittel, Phys. Rev. **73**, 155 (1948).
[20] R. M. Nicklow, N. Wakabayashi, M. K. Wilkinson, and R. E. Reed, Phys. Rev. Lett. **26**, 140 (1971).
[21] Z. Zhang and P. C. Hammel, Appl. Phys. Lett. **68**, 2005 (1996).
[22] A. K. Geim, S. V. Dubonos, J. G. S. Lok, I. V. Grigorieva, J. C. Maan, L. Theil Hansen, and P. E. Lindelof, Appl. Phys. Lett. **71**, 2379 (1997).
[23] P. Rhodes and G. Rowlands, Proc. Leeds Philos. Lit. Soc., Sci. Sect. **6**, 191 (1954).
[24] D. Craik, *Magnetism: Principles and Applications* (Wiley, New York, 1995).
[25] F. C. Rossol and R. V. Jones, J. Appl. Phys. **37**, 1227 (1966).
[26] T. K. Wagner and J. L. Stanford, Phys. Rev. B **5**, 1876 (1972).
[27] B. R. Cooper, R. J. Elliott, S. J. Nettel, and H. Suhl, Phys. Rev. B **127**, 57 (1962).
[28] S. Legvold, J. Alstad, and J. Rhyne, Phys. Rev. Lett. **10**, 509 (1963).
[29] D. N. Lawton, A. Nogaret, S. J. Bending, D. K. Maude, J. C. Portal, and M. Henini, Phys. Rev. B **64**, 033312 (2001).
[30] B. A. Kalinikos and A. N. Slavin, J. Phys. C **19**, 7013 (1986).
[31] R. I. Joseph and E. Schlomann, J. Appl. Phys. **36**, 1579 (1965).
[32] C. Bayer, S. O. Demokritov, B. Hillebrands, and A. N. Slavin, Appl. Phys. Lett. **82**, 607 (2003).
[33] D. Heitmann and U. Mackens, Phys. Rev. B **33**, 8269 (1986).
[34] L. Zheng, W. L. Schaich, and A. H. MacDonald, Phys. Rev. B **41**, 8493 (1990).